

Evidence for anti-synergism between ion-assisted etching and in-plasma photoassisted etching of silicon in a high-density chlorine plasma

Cite as: J. Vac. Sci. Technol. A **38**, 023009 (2020); doi: [10.1116/1.5138189](https://doi.org/10.1116/1.5138189)

Submitted: 13 November 2019 · Accepted: 10 January 2020 ·

Published Online: 30 January 2020



Emilia W. Hirsch, Linfeng Du, Demetre J. Economou,^{a)} and Vincent M. Donnelly^{b)}

AFFILIATIONS

Plasma Processing Laboratory, Department of Chemical and Biomolecular Engineering, University of Houston, Houston, Texas 77204

Note: This paper is part of the Special Topic Collection Commemorating the Career of John Coburn.

^{a)}Electronic mail: economou@uh.edu

^{b)}Electronic mail: vmdonnelly@uh.edu

ABSTRACT

Etching of p-Si in 60 mTorr 10%Cl₂/90%Ar Faraday-shielded inductively coupled high density plasmas was investigated under both ion-assisted etching (IAE) and photoassisted etching (PAE) conditions. Real-time etching rates and after-etching Si surface chemical compositions were obtained by laser interferometry and vacuum-transfer x-ray photoelectron spectroscopy (XPS), respectively. Precisely controlled ion energy distributions (IEDs) were generated by applying pulsed negative DC bias on the conductive sample stage. Above a 36 eV threshold at a total flow rate of 250 SCCM, the IAE rate increased with the square root of the ion energy. In contrast to the DC bias, etching under RF bias did not exhibit a threshold ion energy because of the wide IED. XPS spectra revealed that the surface layer under PAE conditions had a significantly lower chlorine content, composed of only SiCl. Under IAE conditions, however, silicon dangling bonds (Si•), SiCl₂, and SiCl₃ were found on the surface, in addition to SiCl, with a relative abundance of SiCl > SiCl₂ > SiCl₃. The absence of higher chlorides and Si• under PAE conditions suggested that vacuum ultraviolet photons and above threshold-energy ions interact with the surface very differently. By varying the duty cycle of the pulsed DC bias, it was found that the IAE rate scaled with the energetic ion dose, but only for low duty cycles. For higher duty cycles, the apparent IAE yield fell off with an *increasing* Cl coverage on the surface, as the duty cycle went up, which pointed to a negative synergy (antisnergism) between PAE and IAE as the explanation. This antisnergism was further supported by the observed decrease of the total etching rate with an increasing period of the pulsed DC bias. A plausible mechanism is that increasing the pulsing period causes more near-surface damage, creating more recombination centers that lead to a higher loss rate of electron-hole pairs through recombination, thereby reducing the PAE rate.

Published under license by AVS. <https://doi.org/10.1116/1.5138189>

I. INTRODUCTION

Plasma etching continues to play a critical role in the fabrication of ultra-large-scale integrated circuits with device dimensions in the nanoscale and even the atomic scale. To a large extent, this is because directional ions bombarding the substrate give rise to anisotropic etching profiles and high fidelity pattern transfer. This ion-assisted etching (IAE) occurs through a synergy between ions and neutrals. Ion bombardment promotes reactions of chemisorbed neutrals with the substrate atoms, resulting in the formation of products that desorb.¹ Although great progress has been made through separate control of ion energy and flux, as well as the

neutral-to-ion flux ratio, great challenges still remain as the critical dimension of devices approaches the atomic scale.²

In-plasma photoassisted etching (PAE) of p-type Si was first reported by Shin *et al.* in a Faraday-shielded pulsed inductively coupled Cl₂/Ar plasma with nearly monoenergetic ion energy distribution (IED).³ It was found that etching rates increased with the square root of the ion energy above the observed threshold of 16 eV. When the ion energy was below the IAE threshold, an unexpected substantial etching rate was observed, independent of ion energy, which was shown to be induced mainly by the native vacuum ultraviolet (VUV) photons generated in the plasma. More recently, Zhu *et al.* measured the relative etching rates of silicon in

different halogen containing plasmas.⁴ PAE rates were found to be lowest in 50%Br₂/50%Ar plasma and highest in 25%HBr/25%Cl₂/50%Ar plasma. In all cases, the etching rate scaled with the product of halogen surface coverage [measured by x-ray photoelectron spectroscopy (XPS)] and optical emission intensity (Ar 7504 Å, a proxy for VUV emission). The dependence of PAE on the wavelength was investigated by measuring the etching rate of silicon placed under windows with different light transmission characteristics. It was found that photons with a wavelength <120 nm are much more effective in inducing etching. Potential mechanisms of PAE were studied by Sridhar *et al.*⁵ Photoassisted etching (outside of a plasma) had previously been attributed to the creation of electron-hole (e-h) pairs and reactions of these carriers at the surface,^{6,7} the enhancement of photodesorption,⁸ and the surface damage induced by VUV photons, facilitating etching.^{8,9} By modulating the plasma power between two different values at a rate that was much faster than that required to remove a silicon monolayer, the damage-induced mechanism of in-plasma PAE was ruled out.

Up until recently, very few investigators had reported on the possible synergy of radicals, ions, and photons originating from the same plasma. Fukasawa *et al.* demonstrated photoenhanced etching of hydrogenated silicon nitride (SiN_x:H) films in fluorocarbon plasmas.^{10,11} Modification of surface morphology, attributed to plasma-generated VUV photons, was also reported. Enhanced surface roughness was observed due to synergy among VUV photons, ion bombardment, and heating of plasma-exposed 193 nm photoresist by Nest *et al.*¹² Pargon *et al.* found VUV light (110–210 nm) to be the main contributor to the decreased linewidth roughness of the 193 nm photoresist after plasma etching.¹³ Simultaneous irradiation by UV photons resulted in a decreased surface roughness of GaN etched in chlorine plasmas.¹⁴ Tian and Kushner discussed the control of relative fluxes of ions and VUV photons through pressure, pulsed power, gas mixture, and wall condition in low-pressure inductively coupled plasmas using model predictions.^{15,16}

Depending on the application, PAE can be advantageous or an unwanted complication. For example, PAE was used to perform extremely selective etching of nanoholes in silicon using the native oxide as a mask.^{17,18} On the other hand, PAE can be a problem for self-limited atomic layer etching where very low ion energies are used (to promote selectivity), for which the non-self-limiting PAE rate is comparable to the IAE rate.¹⁹ In any case, it is important to understand the nature of plasma-surface interactions, specifically the role played by VUV photons. A mechanistic insight into photoassisted etching could provide clues on how to enhance or reduce PAE relative to IAE.

In this work, etching of p-type Si in Cl₂/Ar Faraday-shielded inductively coupled high density plasmas was investigated under conditions where the ion energy could be precisely controlled resulting in a clear transition from IAE to PAE. Vacuum-transfer XPS and laser interferometry were employed to study the near-surface chemical composition and measure *in situ* and in real-time the etching rate of Si, respectively. The relative importance of IAE compared to PAE was controlled by varying the level and duty cycle of a pulsed negative DC bias applied on the conductive substrate holder. A major goal of this study was to shed light upon any possible synergy during the in-plasma simultaneous bombardment

of silicon by energetic (i.e., above threshold-energy) ions and photons, especially those in the VUV wavelengths.

II. EXPERIMENT

The experimental apparatus consisted of a plasma etching reactor (Fig. 1) and an XPS system. The Faraday-shielded inductively coupled plasma (ICP) was powered by an air cooled four-turn copper coil and has been described in detail previously.³ Radio frequency (RF) power at 13.56 MHz was delivered to the plasma by an RF amplifier (ENI A500) that was driven by a function generator (KEYSIGHT 33600A) with a Π-matching network in a continuous wave (cw) mode. The matching network was manually tuned to maintain a constant net power of 350 W with a reflected power of ~4 W measured with inline Bird watt-meters. A Faraday shield prevented capacitive coupling between the high voltage end of the coil and the plasma, as verified by a very small measured peak-to-peak voltage of ~1.5 V on an electrically floating stage immersed in the plasma, indicating a negligible RF component of the plasma potential.

The chamber was evacuated by a 300 l/s turbomolecular pump, and the base pressure in the plasma source was

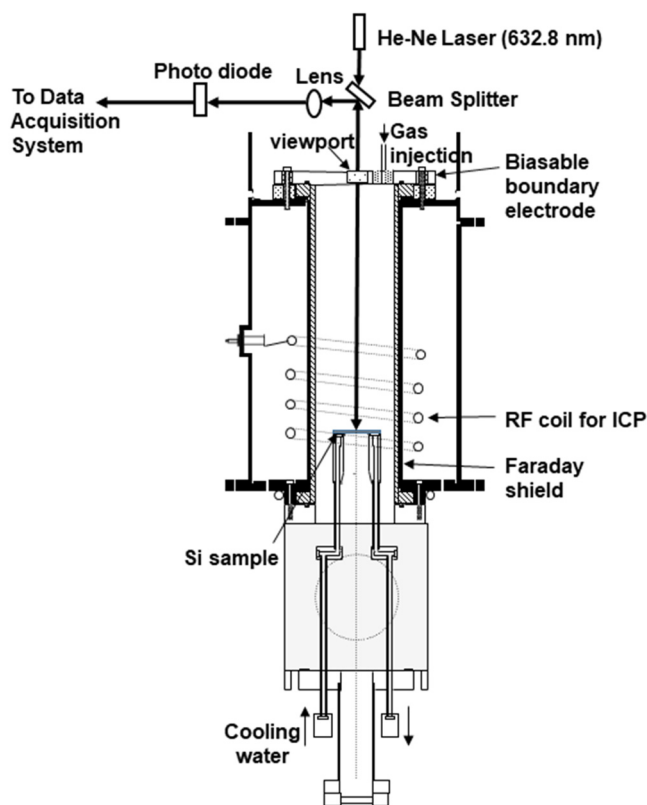


FIG. 1. Schematic of the plasma reactor, with a Faraday-shielded inductively coupled plasma source. An He-Ne laser interferometry setup provided real-time etching rate measurements. Processed samples could be transferred under vacuum to an XPS chamber (not shown) for surface analysis.

$\sim 4 \times 10^{-7}$ Torr. A Cl_2/Ar (molar ratio 1:9) gas mixture was fed through the electrically grounded top flange. A total flow of 50 SCCM (henceforth called “low flow rate”) or 250 SCCM (henceforth called “high flow rate”) was used. The pressure downstream of the ICP source was monitored with an MKS capacitance manometer. Pressure above the sample (corrected for the pressure drop between the sample location and the point where the pressure measurement was made) was maintained at 60 mTorr during etching using a throttle valve. At this pressure, with no bias applied to the sample, it is expected that very few ions will have energy above the ion-assisted etching threshold of silicon.

The water-cooled (20 °C) stainless steel (SS) sample stage was grounded or powered by either a cw RF bias voltage or a pulsed negative DC bias. For RF bias, a function generator (SRS D345) and an amplifier (ENI model A150) were employed to deliver 14.5 MHz power through a Π -matching network. The self-bias voltage was -70 or -140 V with 8 or 20 W, respectively, of RF power applied to the sample stage. Pulsed negative DC bias was applied by amplifying (AVTECH) a negative voltage square wave pulse (BNC 645) with a frequency of 10 kHz. The ion energy with bias ON was assumed to be the difference between the plasma potential (V_p) and the bias voltage, with $V_p = 5$ V at 60 mTorr.⁴

The etching rate experiments were performed using SiO_2 (1 μm thick) masked p-type Si (100) substrates with resistivity 5–100 Ωcm . XPS surface characterization was performed using p-type Si (100) substrates with resistivity 10–20 Ωcm . Si wafers were cleaved into $\sim 1.1\text{cm}^2$ square pieces, cleaned with acetone and methanol to remove carbon contaminants and blown dry with nitrogen. Native oxide was removed by etching with a high bias for a few seconds before PAE started. The face of the 2.54 cm-diameter SS sample holder was covered with a 1.95 cm-diameter highly doped p-type Si disk (resistivity 0.001–0.005 Ωcm), soldered with indium foil, to prevent metal contamination due to SS sputtering. Low Si disk resistivity and indium soldering under a dry N_2 purge were found to be essential to minimize the voltage drop between the DC power supply and the surface of the Si disk. Samples were bonded to the Si disk using either silver paste (Mung II) for XPS measurements or indium foil for etching rate measurements to ensure good thermal and electrical contact. In addition, the back sides of both the sample and the Si disk were scribed by a diamond tip to break the native oxide to help in making good electrical contact. To make sure there was minimum corrosion of the indium (and loss of electrical contact), the voltage difference between the sample surface and the applied negative DC bias was measured before and after etching in seven separate cases and was found to be 7 ± 3 V. This was accounted for in obtaining the actual DC bias seen by the sample.

Previously, a temperature rise of ~ 200 °C was observed after a few minutes of etching Si with -50 V DC sample bias when the samples were not thermally bonded to the water-cooled stage.³ The temperature of the substrate was not measured in the present study; however, with a much better thermal contact between the sample and the water-cooled stage, the temperature rise is expected to be much less. In addition, data were collected in a random order to minimize systematic errors due to any temperature dependences, which are expected to be small, as well as any other adverse effects.

Real-time etching rates were measured by laser interferometry.^{20–22} A 632.8 nm He-Ne laser beam at normal incidence was reflected off the sample and detected with a photodiode. The signal was digitized and recorded with a LABVIEW program. The pitch width (line + space) of the SiO_2 mask pattern was 100 μm at 50% density. Interference between reflections off the masked and unmasked regions caused the intensity of the reflected beam to oscillate as a function of time with a period corresponding to an etching depth $\Delta d = \lambda/2$, where λ is the laser wavelength. Interference persisted until the SiO_2 mask was slowly etched away or the increased surface roughness led to significantly low reflected beam intensity. To evaluate possible errors introduced by etching of the SiO_2 mask, the etching rate of blanket SiO_2 using either RF bias or pulsed negative DC bias was also obtained by either laser interferometry or spectroscopic ellipsometry (J. A. Woollam M-2000).

After etching, the sample was transferred under vacuum to an ultrahigh vacuum ($\sim 6 \times 10^{-10}$ Torr base pressure) analysis chamber equipped with an XPS system (Surface Science Instruments M-Probe), with a monochromatic Al $K\alpha$ x-ray source at 1486.6 eV. Measurements were carried out at take-off angles (with respect to the sample plane) of 30° and 85° with probing depths of 11 and 22 Å, respectively.²³ Photoelectrons from the sample were collected with a hemispherical kinetic energy analyzer having a $\pm 15^\circ$ acceptance cone. Low resolution XPS spectra were recorded over 0–1000 eV, and the integrated intensities of the core-level peaks were used to determine the elemental composition and total chlorine content of the surface. High resolution spectra of the Si (2p) region from 95 to 105 eV were also recorded to determine the stoichiometry of the chlorinated surface. Samples were etched for ~ 1000 Å based on the etching rate measured before XPS analysis. The simultaneous cessation of both source and bias power defined the end of the etching period²⁴ and established the conditions of the film that was subsequently analyzed by XPS.

III. RESULTS AND DISCUSSION

A. Etching rates

Real-time etching rates measured by laser interferometry for p-Si in 60 mTorr 10% Cl_2 /90%Ar plasmas with SiO_2 masked patterned samples are plotted as a function of the square root of ion energy in Fig. 2. RF bias (black squares for the low flow rate and magenta stars for the high flow rate) or pulsed negative DC bias with 50% duty cycle at a frequency of 10 kHz (solid red circles for the low flow rate and open red circles for the high flow rate) was applied to the sample stage during etching. Ion energy was taken as the difference between the plasma potential ($V_p \sim 5$ V) and the applied negative DC bias or the self-bias when the stage was powered with RF. At 60 mTorr, ions would suffer collision with probability, $P = 1 - \exp(-s/\lambda)$, of 12% and 27% while traversing the sheath at -30 and -100 V bias, respectively, with corresponding sheath thickness (s) of ~ 110 and ~ 260 μm estimated based on the Child law sheath model and a mean free path (λ) of ~ 830 μm . Therefore, ion collisions in the sheath produced only a small broadening of the IED, preserving (in the case of applied DC bias) an essentially monoenergetic IED.

Etching rates under pure PAE conditions were measured with the sample stage grounded, so the ion energy was equal to V_p .

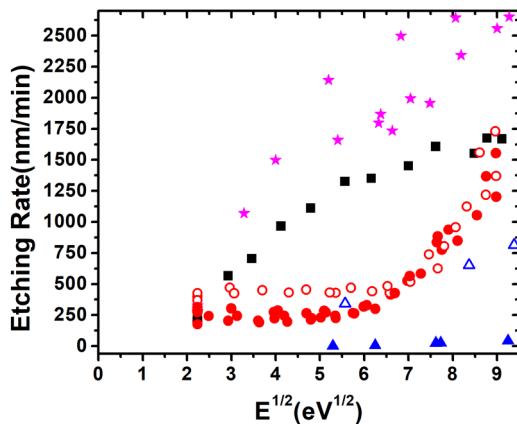


FIG. 2. Etching rates of p-Si as a function of $E^{1/2}$ (E = ion energy) with the application of either RF bias (black squares for the low flow rate and magenta stars for the high flow rate) or pulsed negative DC bias at 10 kHz and 50% duty cycle (solid red circles for the low flow rate and open red circles for the high flow rate). Etching rates of SiO_2 for the low flow rate under pulsed negative DC bias at 10 kHz, with 50% duty cycle (blue solid triangles) or RF bias (blue hollow triangles) are also shown.

Etching rates of blanket SiO_2 films were also obtained by either laser interferometry (ion energy of ~ 60 or ~ 85 V) or spectroscopic ellipsometry (ion energy of ~ 30 or ~ 40 V) by measuring the film thickness change after 5 min of etching under pulsed negative DC bias at 10 kHz and 50% duty cycle (blue solid triangles) or RF bias (blue hollow triangles).

As shown in Fig. 2, under pulsed DC bias, SiO_2 starts to etch slowly when the ion energy is ~ 60 eV. The etching rate is ~ 25 nm/min at 60 eV and ~ 40 nm/min at 85 eV. The etching rate of SiO_2 under RF bias is much higher ~ 650 nm/min at 60 eV and ~ 810 nm/min at 85 eV. The significantly lower etching rate of SiO_2 under pulsed DC bias compared to that under RF bias is likely due to charging of the insulating SiO_2 mask. Since SiO_2 etching rates with pulsed DC bias are much lower than the Si etching rates, SiO_2 etching has likely no contribution to the laser interferometry signal used to determine the silicon etching rate with DC bias. Under RF bias, however, the fast etching of SiO_2 is likely due to the very wide ion energy distribution caused by the thin sheath at this high plasma density. This SiO_2 etching would lead to a moderate underestimation of the Si etching rates, especially for higher ion energies.

Estimating an ion flux of $\sim 1.4 \times 10^{17} \text{ cm}^{-2} \text{ s}^{-1}$ from the measured ion current density at the substrate (see below), the SiO_2 mask will charge up to ~ 0 V potential above $\sim 10\%$ duty cycle for -60 V pulsed DC bias (see the Appendix). Ions may be deflected near the mask edge resulting in nonuniform etching across the bottom of the trench. Most of the trench bottoms were found (by SEM) to be flat after etching; hence, mask charging did not affect the measured Si etching rates. Etching under RF bias yielded vertical sidewalls (no taper), implying as expected that charging was also not an issue under RF bias.

The Si etching rates measured with RF bias (Fig. 2) scale roughly with the square root of ion energy without showing a

threshold. This is due to the bimodal IED that occurs when the period of the applied RF bias is longer than the ion transit time through the sheath, resulting in ions responding to the changing sheath voltage.²⁵ The peak separation of the Ar^+ bimodal IED reported by Hoekstra and Kushner in a low-pressure (10 mTorr) Ar/ Cl_2 ICP was ~ 50 eV, for a self-bias voltage of -31 V on the substrate under 13.56 MHz RF bias.²⁶ The high energy ions in this broad IED would smear out the threshold that otherwise would appear at the low ion energy end. This shows a clear advantage offered by pulsed DC bias, which provides a better control of IED, and thereby a clearer separation between PAE and IAE. Of course, DC bias can be effective only when both the substrate holder and the sample are conductive.

In contrast to the RF bias case, IAE threshold energies (~ 25 eV for the low flow rate and ~ 36 eV for the high flow rate experiments) are clearly seen when pulsed negative DC bias is applied to the sample stage. Below the threshold, etching is induced by VUV photons, and the etching rate under the PAE condition (with the sample stage grounded) is ~ 300 nm/min for the low flow rate and ~ 400 nm/min for the high flow rate. The lower PAE rate at the low flow rate may be due to a “loading effect” that results in depleted Cl number density, relative to the higher flow rate. Assuming all of the Si exposed to the plasma (including the exposed edges of the underlying disk) is etching, and the product is SiCl_4 , only 1.6% of the Cl_2 feed gas is consumed at the high flow rate for an etching rate of 400 nm/min. Cl_2 consumption would rise to 8.2% for the low flow rate at this etching rate. If the PAE rate scaled with Cl and Cl_2 number density, then the low flow rate PAE rate would drop no lower than 370 nm/min. The drop to the observed 300 nm/min at the low flow rate indicates that additional changes with the flow rate, such as a modest decrease in VUV intensity, are also occurring. At the highest ion energy investigated, the etching rate is about the same (~ 1600 nm/min) at high and low Cl_2 flow rates, while the Cl_2 consumption is 7% and 32%, respectively. This trend is also not explained by the loading effect and suggests that IAE is limited by ion flux and not neutral flux.

Figure 2 also shows that, above the threshold, the etching rate under DC bias scales with $E^{1/2}$ as reported in other studies.^{27–30} Table I summarizes the threshold values of IAE of Si with chlorine. The reported thresholds range from 9 to 45 eV depending on the conditions. The threshold energies observed in this work are consistent with some of the studies in Table I, including our previous study⁴ under similar conditions. In the present study, considering the lower ionization potential of Cl versus Ar, the 9:1 flow rate ratio between Ar and Cl_2 , and the expected high percent dissociation of Cl_2 at the high power density employed, the densities of Ar^+ and Cl^+ are likely roughly equal, with little Cl_2^+ , consistent with model predictions for somewhat different conditions.³¹ The conditions in the present study most closely match those of Sawin and co-workers, who reported much lower thresholds of 16 or 10 eV with an Ar^+ or a Cl^+ ion beam and a Cl/ Cl_2 neutral beam.^{27,28} The apparent discrepancy may be due to the way in which thresholds are defined. In the present study, the threshold corresponds to the ion energy, below which PAE occurs at a constant (no dependence on ion energy), appreciable rate. In the experiments of Sawin and co-workers, the threshold was determined from a linear extrapolation of the plot of etching rate versus the square root of ion energy

TABLE I. Threshold values of ion-assisted etching of Si with chlorine reported in the literature.

Beam or plasma	Species	Material	IAE threshold (eV)	Reference	Other conditions
Beam	Ar ⁺ /Cl or Cl ₂	Undoped poly-Si	16	27	6.2 × 10 ¹⁴ –1.2 × 10 ¹⁶ ions/cm ² /s for ion beam, 1.4 × 10 ¹⁶ –2.8 × 10 ¹⁷ atoms/cm ² /s for atom beam, sample T = 40 ± 5 °C
Beam	Cl ⁺ /Cl or Cl ₂	Undoped poly-Si	10	28	Ion flux 0.1–2 mA/cm ² , IED 10 eV, FWHM 6.2 × 10 ¹⁴ –1.2 × 10 ¹⁶ ions/cm ² /s for ion beam, 1.4 × 10 ¹⁶ –2.8 × 10 ¹⁷ atoms/cm ² /s for atom beam, sample T = 40 ± 5 °C
Beam	Cl ⁺ and Cl ₂ ⁺ /Cl or Cl ₂	Si	9	29	Plasma beam system with a mixture of Cl ₂ ⁺ (70%) and Cl ⁺ (30%) ions, neutral flux Cl ₂ (90%) and Cl (10%)
Beam	Cl ₂ ⁺ /Cl ₂	Poly-Si	25	30	
Beam	Ar ⁺ /Cl ₂	Poly-Si	45	30	
Beam	Ar ⁺ /Cl ₂	Poly-Si	42	32	
Plasma	Ar and 1%–3% Cl ₂	p-Si	16	3	Pulse plasma with synchronous dc bias, 60 mTorr
Plasma	50% Ar and 50% Cl ₂	p-Si	28	4	CW plasma, 60 mTorr
Plasma	90% Ar and 10% Cl ₂	p-Si	25 or 36	This work	CW plasma, 60 mTorr

to the zero etching rate. If PAE occurred in their experiment, this method would have led to a lower apparent threshold than those obtained in the present study.

The IAE yield (number of Si atoms removed per incident ion) at the high flow rate was calculated with the IAE rate (total etching rate minus PAE rate) under pulsed DC bias at 50% duty cycle and 10 kHz. The estimated neutral-to-ion flux ratio under these conditions was ~30, and the energy-selected ion flux was 7 × 10¹⁶ cm⁻² s⁻¹. For 55, 60, and 75 eV ion energies, the etching yield was found to be 0.25, 0.4 and 1.1, respectively. These yields are uncorrected for an apparent suppression of PAE by energetic ion bombardment, as addressed below, and so the actual IAE yields can be up to twice these values at higher ion energies. Given these complexities, the yields found in this work are in reasonable agreement with the values reported by Chang *et al.*, which are 1.2 and 1.7 for 55 and 75 eV Cl⁺/Cl and 0.1 and 0.5 for 35 and 60 eV Ar⁺/Cl.^{27,28}

A central goal of this work was to explore the possibility of synergy between VUV photons and energetic ions, much like the well-known synergy between energetic ions and reactive neutrals in RIE.¹ By employing a pulsed negative DC bias with a variable duty cycle and relatively high frequency (10 kHz), the sample was subjected to etching stimulated by VUV photons only (when the DC bias was OFF) or the sum of VUV photons and energetic ions (when the DC bias was ON). Bias durations of between 0 and 90 μs were used. In 90 μs, only 0.0015 nm of Si (or about 1% of a monolayer) was etched away. This time is also fast compared to the gas average residence time in the reactor (~0.1 s) or diffusion to the walls (~1 ms). Consequently, for a given duty cycle of the applied DC bias, the nature of the surface was the same (i.e., the same silicon chloride composition, subsurface defect density, etc.), and the flux of neutral species to the surface was the same for the portion of the 100 μs period when the bias was ON, as it was for the remainder of the 100 μs period when the bias was OFF. Therefore, by varying the bias duty cycle, the energetic ion flux

averaged over many bias periods was conveniently varied while keeping the neutral flux and VUV photon flux constant. As addressed below, the surface nature and neutral flux could depend on the duty cycle, however, as for example, in the case where the etching rate at high duty cycles becomes large enough to be limited by the supply of neutrals, causing chlorine coverage to falloff.

If the total etching rate with the negative DC bias ON is simply the sum of IAE and PAE rates, then a linear variation of the etching rate as a function of the bias duty cycle is expected. Deviation above or below linearity could indicate positive or negative synergy, respectively, between above threshold-energy ions and VUV photons. An etching rate that increases sublinearly with increasing bias duty cycle could also simply be due to a transition into a neutral-starved regime, an explanation that is inconsistent with the flow rate behavior in Fig. 2 and further discussed below.

Figure 3 presents measurements of the etching rate (black squares) and ion current (blue line and open circles) versus the duty cycle of a 10 kHz –60 V DC bias. Making the PAE rate (the value at 0% duty cycle) the origin of the left y-axis brings out the scaling of IAE rate (total etching rate minus PAE rate) versus duty cycle. The substrate ion current was obtained by measuring the voltage drop across a 200 Ω resistor using an oscilloscope. When negative DC bias is ON, no electron current flows from the plasma to the substrate, and when bias is OFF, the electron and low energy ion currents balance; hence, the detected net current is zero (not shown). The secondary electron emission coefficient reported by Qin *et al.* for Si is 0.74 for Ar⁺ at 500 eV,³³ so with –60 V bias, the effect of secondary electrons should be negligible. In any case, the secondary electron emission current will be proportional to the energetic ion current, so the trend of ion current versus duty cycle will be valid even without correction for secondary electron emission. The energetic ion current integrated over a full period of bias modulation increases nearly linearly with the duty cycle; consequently, the ion current to the surface was a nearly constant ~58 mA within a DC bias pulse (from an extrapolation of the

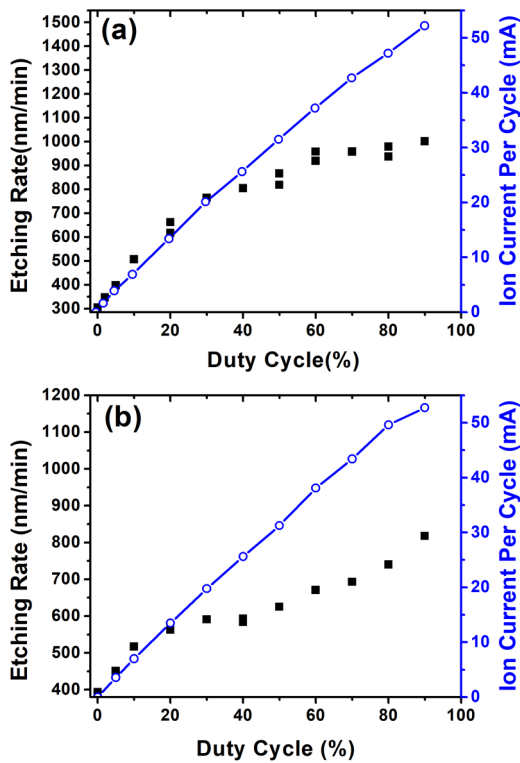


FIG. 3. Total etching rate (including both IAE and PAE) of p-Si as a function of duty cycle with the application of -60 V pulsed DC bias at 10 kHz (black squares) for (a) low flow rate and (b) high flow rate. The PAE rate (0% duty cycle) was set as the origin on the left y-axis. The corresponding integrated energetic ion current per cycle is also shown (blue line and open circles).

currents in Fig. 3 to 100% bias duty cycle). Given the 2.64 cm² area over which the current is collected, this corresponds to an ion flux of 1.4×10^{17} cm⁻² s⁻¹. Note that this is the positive ion flux, regardless of the duty cycle. The *energetic* ion flux (an energy of the 5 V plasma potential plus the absolute value of the DC bias), averaged over many bias periods, is a nearly linearly increasing function of duty cycle and is simply computed from the ion currents in Fig. 3.

At the low flow rate [Fig. 3(a)], the IAE rate increased linearly with an increasing duty cycle (and therefore ion dose), up to about 30%. Above the 30% duty cycle, the IAE rate became sublinear. This could be ascribed to several causes, including neutral-starved conditions and redeposition of etching products. If either of these are the explanation, then a five-time higher Cl₂ flow rate should result in a deviation from linearity at a higher duty cycle or no deviation. The results in Fig. 3(b) show that the deviation from linearity starts at a lower $\sim 20\%$ duty cycle. This effect is attributed to the suppression of PAE by ion bombardment, as discussed below.

It should be noted that the etching rates in Figs. 2 and 3 are higher than those typical of current manufacturing processes for Si etching in chlorine-containing plasmas, using commercial etching tools. These processes are carried out at lower power densities than in the present study, due mainly to the need for radial uniformity

in etching rates. In addition, most of the required etching depths are not large, and, therefore, very fast etching rates are not necessary. When very deep etching is required, SF₆-containing plasmas are usually used. Though uncommon, it is possible to obtain fast etching rates approaching those in the present study. For example, Lane *et al.* reported etching rates of 650 nm/min for a 10 mTorr, 500 W (0.04 W/cm³, $n_e = 3 \times 10^{11}$ cm⁻³ \approx positive ion density³⁴) Cl₂ plasma in a Lam Research model 9400SE transformer-coupled plasma, with 150 W (0.85 W/cm²) RF bias power on a chuck holding 150 mm diameter Si wafers.³⁵ Given the higher volumetric power density (0.40 W/cm³) and higher RF bias power density (2 W/cm²) for the measurements in Fig. 2, the approximately three-fold higher etching rates in the present study are reasonable.

The electron temperature (T_e) measured by a Langmuir probe for a continuously powered, pure Ar plasma at 300 W and 50 mTorr in a similar setup was 2.0 eV.²⁵ The expected T_e for a Cl₂/Ar plasma is lower due to the lower ionization potential of Cl (12.96 eV) compared with Ar (15.8 eV). Assuming $T_e \sim 1.5$ eV in the present study and the ion mass ~ 40 amu for Cl⁺ or Ar⁺, the calculated Bohm velocity is $u_B = 1.9 \times 10^5$ cm/s. Therefore, given the ion flux ($f_+ = 0.6 n_e u_B$) of 1.4×10^{17} cm⁻² s⁻¹, the estimated plasma density is $n_e = 7.0 \times 10^{11}$ cm⁻³ at the sheath edge and $n_e = 1.2 \times 10^{12}$ cm⁻³ in the bulk plasma. This plasma density is several times higher than in commercial processes, such as noted above, again explaining the observed higher etching rates. Because a Faraday shield was required in the present study to obtain well defined ion energy distributions, it was not possible to maintain a plasma at the low density required to slow the etching rate to a value more common in etching processes. Nonetheless, it is possible to apply our findings to these commercial processes by simple scaling of plasma density.

B. Surface chemistry

We also investigated the chemical composition of the chlorinated silicon surface. Table II displays the normalized elemental chemical composition of p-Si (100) derived from XPS low resolution survey spectra at take-off angles of 30° and 85° after etching in a 60 mTorr Cl₂/Ar plasma with the sample stage grounded (PAE condition) or RF powered with -70 and -140 V self-bias voltage at the low flow rate. Besides Si2p (99.6 eV), Si2s (150.9 eV), Cl2p (200.4 eV), and Cl2s (271.8 eV) core-level photoelectron peaks, trace amounts ($<1\%$ of the total Cl concentration) of O1s (533.9 eV) was also detected when RF bias was applied. No other species (e.g., C or metal) were detected. The source of the trace

TABLE II. Normalized elemental composition measured by XPS low resolution survey spectra at take-off angles of 30° and 85° for blanket p-Si after etching in 60 mTorr Cl₂/Ar plasma at low flow rate with the sample stage powered by RF (-70 and -140 V self-bias) or without any bias (0 V, grounded).

	0 V/30°	0 V/85°	70 V/30°	70 V/85°	140 V/30°
Si	84	90	70	81	66
Cl	16	10	29	18	34
O	—	—	1.0	1.6	0.8

O contamination could be from sputtering of the alumina cap that covered the sample stage to prevent metal contamination.

The relative chlorine concentration ($[Cl]/[Si]$) was calculated using

$$[Cl]/[Si] = \frac{A[Cl(2p)]/S[Cl(2p)]}{A[Si(2p)]/S[Si(2p)]}, \quad (1)$$

where $A[Cl(2p)]$ and $A[Si(2p)]$ are the integrated intensities of Cl (2p) and Si(2p) peaks of low resolution survey spectra and $S[Cl(2p)]$ and $S[Si(2p)]$ are the corresponding sensitivity factors²³ (2.285 and 0.817), respectively. Both 2p spin-orbit components were included in the integration. The relative chlorine concentration is plotted as a function of the ion energy ($V_p - \text{bias voltage}$) in Fig. 4. When the take-off angle (with respect to the sample surface) increases (red circle for 85°), the relative chlorine signal decreases, indicating that the chlorinated layer is mostly located at the uppermost surface and its thickness is comparable to the electron inelastic mean free path.²³

The relative chlorine concentration increases with increasing bias voltage, as reported previously by Layadi *et al.*²³ The highest ion energy (145 eV for -140 V self-bias) leads to the highest relative Cl concentration (0.52 at 30°) compared to 0.41 at 30° with ion energy of 75 eV. On the other hand, the lowest Cl content was observed under PAE conditions (ion energy ~ 5 V), resulting in a relative concentration of 0.19 at 30° and 0.11 at 85°. Consequently, the nature of the chlorinated layer under PAE without any energetic (above threshold-energy) ion bombardment appears to be very different from that of IAE.

High resolution Si(2p) spectra were also recorded to determine the nature of the chlorinated layer after etching. Figure 5 shows the spectra of the Si(2p) peak with the sample stage grounded (PAE) or RF biased (-70 or -140 V self-bias) at take-off

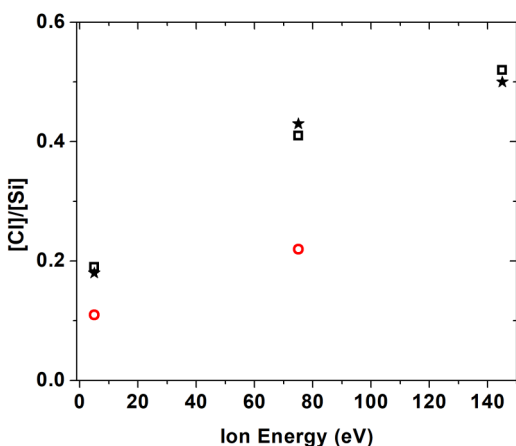


FIG. 4. Relative chlorine concentration after etching in 60 mTorr Cl_2/Ar plasma obtained from XPS survey spectra at take-off angles of 30° (black squares) and 85° (red circles) at the low flow rate. Black stars were calculated based on the integrated areas of deconvoluted $SiCl_x$ peaks obtained by high resolution XPS at 30° (see below).

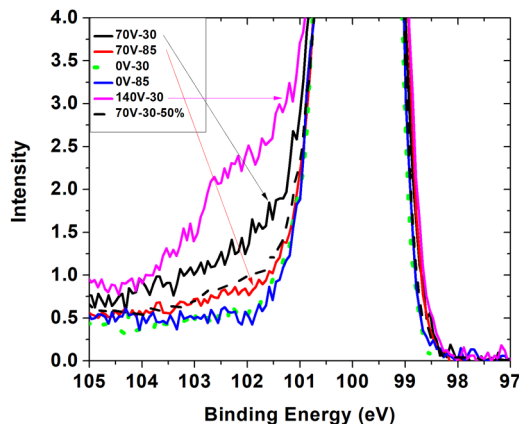


FIG. 5. High resolution Si(2p) spectra at take-off angles of 30° or 85°. Etching conditions were 0 V (PAE), RF at -70 V self-bias, and RF at -140 V self-bias, all at the low flow rate. Intensities were normalized at the maximum near 100 eV. The black dashed line is from a sample etched under pulsed -70 V DC bias with 50% duty cycle at 10 kHz, also at low flow rate.

angles of either 30° or 85° at the low flow rate. All spectra have been shifted to a common binding energy and normalized to the peak intensity of the -70 V spectrum at 30°. At the 85° take-off angle, the chloride tails are less intense on the high binding energy side (101–104 eV) for both -70 V (red) and 0 V (blue) as compared with those at 30° (black and green) indicating that most Cl bonded to Si is confined to the surface. Higher ion energy (larger bias) enhances the signals at high binding energy, which is consistent with the higher chlorine content derived from the low resolution survey spectra. Most importantly, a significant difference of the Si(2p) peak on the high energy side (101–104 eV) was observed between etching under PAE condition without bias (green) and IAE condition under RF bias (black for -70 V self-bias, magenta for -140 V self-bias), which is discussed below. In addition, the Si(2p) peak increasingly broadens on the lower energy side with increasing ion energy, showing a weak shoulder. This is due to the creation of Si dangling bonds by ion bombardment when the ion energy is above threshold.²³

Deconvoluted high resolution Si(2p) spectra (Fig. 6) were obtained by peak fitting for various bias voltages (0, -70 , and -140 V). Deconvolution employed a Shirley-shaped background and assumed a spin-orbit splitting of 0.61 eV and an intensity ratio ($2p_{3/2}/2p_{1/2}$) of 1.92 (Refs. 36 and 37) with 95% Gaussian and 5% Lorentzian line shapes. Binding energies, peak intensity, and peak widths were constrained in a minimal fashion. Excellent fits of Si(2p) spectra were obtained for all three cases with minimal χ^2 values between the fitted spectra (dark yellow line) and the experimental data (black squares).

After etching under the IAE condition with RF power on the sample stage [-70 V self-bias: Fig. 6(b); -140 V self-bias: Fig. 6(c)], much broader chloride tails appear from 101 to 104 eV, and the high resolution Si(2p) peak can be deconvoluted into five individual peaks. These peaks are attributed to Si with a dangling bond ($Si\cdot$), $Si(\text{bulk})$, $SiCl$, $SiCl_2$, and $SiCl_3$, respectively, in agreement

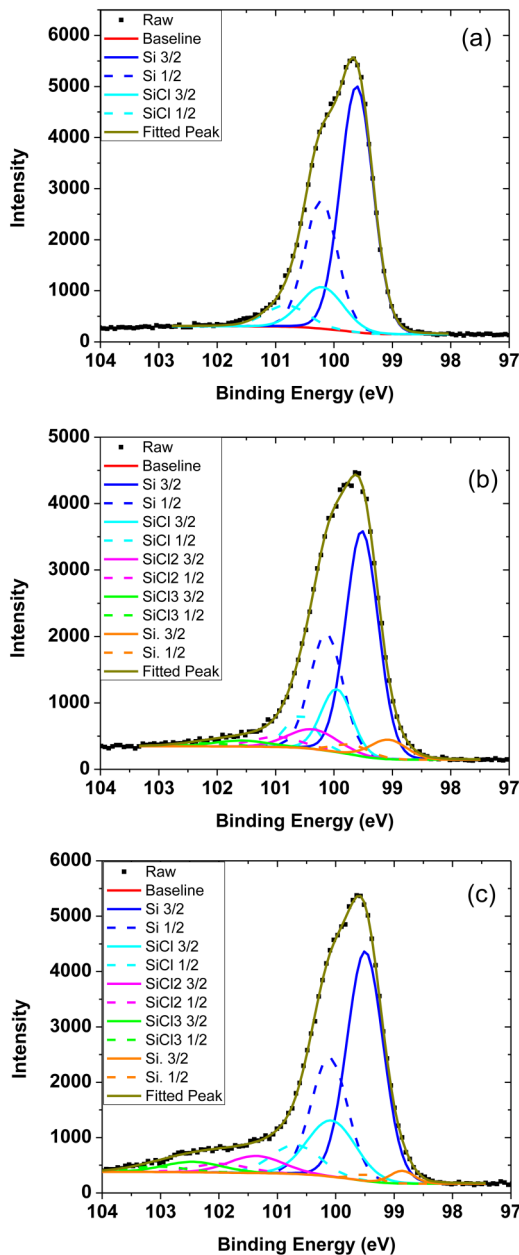


FIG. 6. Peak fitting of high resolution Si(2p) spectra at a take-off angle of 30°. Etching conditions were (a) 0 V (PAE), (b) RF, -70 V self-bias, and (c) RF -140 V self-bias, all at the low flow rate.

with earlier studies by Layadi *et al.*²³ and Bogart and Donnelly.³⁸ The binding energies of the 2p_{3/2} component with -140 V self-bias [Fig. 6(c)] are 98.8 (Si•), 99.5 (bulk Si), 100.1 (SiCl), 101.4 (SiCl₂), and 102.5 eV (SiCl₃), respectively. On the other hand, after etching under PAE condition, only two individual peaks can be identified by fitting the high resolution Si(2p) peak [Fig. 6(a)]: one

corresponding to the two spin-orbit components of Si(bulk) at 99.6 eV and the other ascribed to SiCl at 100.2 eV. This dramatic difference of missing higher chlorides (SiCl₂ and SiCl₃) and Si with a dangling bond (Si•) under PAE condition is a clear indication that VUV photons and energetic ions are interacting with the Si surface very differently. The most likely explanation is that energetic ion bombardment disrupts the surface and subsurface, leading to the formation of higher chlorides, while VUV light does not.

The relative chlorine concentration was also calculated based on the integrated area of individual deconvoluted SiCl_x peaks of the high resolution Si(2p) peak²³ given by

$$[\text{Cl}]/[\text{Si}] = \frac{A[\text{SiCl}] + 2A[\text{SiCl}_2] + 3A[\text{SiCl}_3]}{(A[\text{Si}] + A[\text{Si}_k] + A[\text{SiCl}] + A[\text{SiCl}_2] + A[\text{SiCl}_3])}, \quad (2)$$

The calculated relative chlorine concentrations were 0.18, 0.43, and 0.50 for 0, -70, and -140 V (solid black stars in Fig. 4), respectively. There is good agreement between the values of [Cl]/[Si] derived from the low resolution survey spectra (black hollow squares in Fig. 4) and the high resolution spectra. This also justifies the overall validity of the peak fitting procedure.

After etching under the PAE condition, the near-surface region of Si (100) that consists of a chlorinated SiCl layer with higher chlorides absent is similar to the surface of trench sidewalls after etching, observed by Bogart and Donnelly.³⁹ This is reasonable because (energetic) ion bombardment is absent for both the sample surface under the PAE condition and the trench sidewalls during reactive ion etching. In contrast, with bias voltage applied, the chlorinated layer contains additional components including Si dangling bonds, SiCl₂, and SiCl₃. The integrated area of these SiCl_x (x = 1–3) components shows that the ordering of their relative abundance is SiCl > SiCl₂ > SiCl₃, and the corresponding ratios are 1:0.50:0.17 at -70 V and 1:0.34:0.23 at -140 V self-bias, under RF biasing of the sample stage.

We also investigated the surface chemistry after etching with alternating IAE and PAE by varying the DC bias pulse duty cycle. As shown in Fig. 7, the chlorine coverage rises quickly with very little ion bombardment (less than 10% duty cycle) added for both high and low flow rates, then turns over and rises slowly. The slightly higher Cl coverage at the low flow rate is just within the uncertainty of the measurement. Etching under a pulsed -70 V DC bias at 10 kHz gave a relative Cl concentration of 0.28 at a 50% duty cycle at the low flow rate, which is ~30% lower than the value (0.41) obtained under RF power (-70 V self-bias) applied continuously on the sample stage. The corresponding chloride tail between 101 and 104 eV of the high resolution Si(2p) peak in Fig. 5 (black dashed line) is also substantially smaller than that with RF bias at the same bias voltage (black solid line) and much larger than that after etching under the PAE condition (green dotted line). This is reasonable, since a bimodal energy distribution is obtained with RF bias, and higher energy ions are more efficient in creating chlorination sites.

C. Mechanism

Assuming nearly complete dissociation of Cl₂, and a gas temperature similar to a 6 mTorr Cl₂ plasma (600 K),⁴⁰ at the high flow rate (where little chlorine is present as SiCl_x), the Cl number

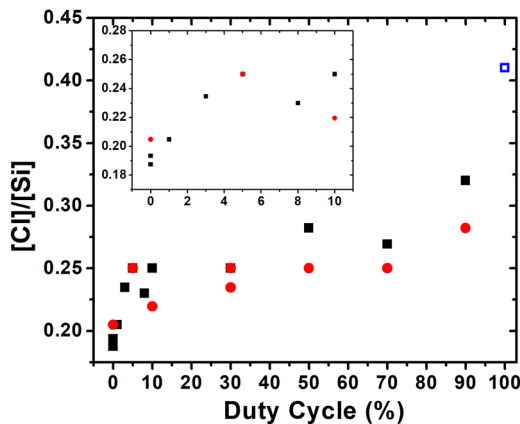


FIG. 7. Relative chlorine concentration obtained from XPS survey spectra at a take-off angle 30° . Etching conditions were RF -70 V self-bias (blue open square) and pulsed -70 V DC bias at 10 kHz for the low flow rate (black solid squares) and the high flow rate (red solid dots). The inset is an enlargement of the region with a duty cycle less than 10% .

density is $\sim 2 \times 10^{14}\text{ cm}^{-3}$, corresponding to a flux of $\sim 2 \times 10^{18}\text{ cm}^{-2}\text{ s}^{-1}$. Therefore, when the DC bias is ON continuously, the Cl-to-ion flux ratio, f_{Cl}/f_+ , is ~ 15 , while for 5% duty cycle, f_{Cl}/f_+ , is ~ 240 . Here, the ion flux was taken to be $1.4 \times 10^{17}\text{ cm}^{-2}\text{ s}^{-1}$ as estimated above. Si yields derived from the data in Fig. 3(b) at the high flow rate are presented in Fig. 8. Given the small rate of consumption of Cl_2 at the maximum etching rate

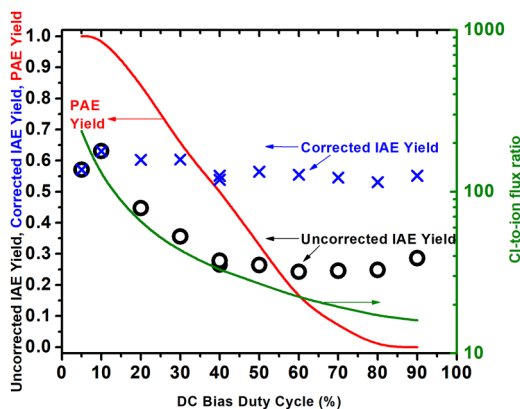


FIG. 8. Etching yields as a function of pulsed DC bias duty cycle, derived from the measurements in Fig. 3(b) for the high flow rate case. The uncorrected ion-assisted etching yields (black open circles) are simply the observed etching rates (Si atoms/ $\text{cm}^2\text{ s}^{-1}$) divided by the positive ion flux obtained from the measured ion currents. The photoassisted etching relative yield (red line) was assumed to smoothly transition from zero in the limit of zero Cl-to-ion flux ratio (f_{Cl}/f_+), to unity at very high f_{Cl}/f_+ values (see text). The corrected IAE yields (blue \times s) account for a declining PAE etching rate as f_{Cl}/f_+ decreases with increasing bias duty cycle. Estimated f_{Cl}/f_+ values as a function of bias duty cycle are also included (green line).

at the high flow rate, these measurements are considered to represent a simpler case in which the ion flux (mainly a mix of Ar^+ and Cl^+) and neutral flux (mainly Cl , with little Cl_2 or SiCl_x) are better defined than at the low flow rate.

Computing the ion-assisted etching yield from the observed [Fig. 3(b)] total etching rate minus the photoassisted etching rate, the latter in the absence of substrate bias, results in the open circles in Fig. 8 (labeled uncorrected IAE yields). Etching yields increased from 0.29 to 0.36 to 0.60 as f_{Cl}/f_+ increased from 16 to 40 to 240. Chang and Sawin have reported Si etching yields of ~ 1.2 , 2.5, and 3.1 at these Cl-to- Cl^+ flux ratios for 75 eV ions.²⁸ When Ar^+ was used instead of Cl^+ , Si yields of ~ 0.5 , 1.0, and 1.8 were found at the same respective Cl-to- Ar^+ flux ratios at an ion energy of 60 eV .²⁷ The yields in the present study are lower than the reported values, but the relative trend in yield versus neutral-to-ion flux ratio is in reasonable agreement with these prior studies. Furthermore, the etching rate in the present study at 90% duty cycle is about half that expected from a linear extrapolation of the 20% duty cycle value [Fig. 3(b)]. As discussed above, ascribing this behavior to a too-low Cl-to-ion flux ratio is inconsistent with the flow rate dependence in Fig. 3.

In addition, this explanation leads to a further inconsistency. The etching yield should be independent of ion flux and increase with the concentration of chlorine in the near-surface region. Chang *et al.* found that the yield increased with increasing f_{Cl}/f_+ , but was independent of ion flux for a given f_{Cl}/f_+ . They also attributed the increase and then saturation of the etching yield with increasing f_{Cl}/f_+ to the increasing chlorine coverage, but no measurements were made of chlorine coverage versus f_{Cl}/f_+ . The XPS measurements in the present study, shown in Fig. 7, are in conflict with this conclusion. Cl coverage increases by $\sim 20\%$ as f_{Cl}/f_+ decreases from ~ 300 (at a duty cycle of $\sim 3\%$) to 15 (at a duty cycle of 100% , i.e., cw). This would lead to the unreasonable conclusion that the ion-assisted etching yield decreases as chlorine coverage increases, and furthermore the yield when most surface chlorine is in the form of SiCl_2 and SiCl_3 is lower when chlorine is present solely as SiCl .

We therefore conclude that the IAE yield should be nearly independent of f_{Cl}/f_+ for the conditions in the present study. The only way this is possible is if ion bombardment suppresses the photoassisted etching process. In the limit of very high f_{Cl}/f_+ (i.e., for small DC bias duty cycles), there is no suppression and the relative PAE yield (normalized to the value at zero duty cycle) is unity. At the opposite limit of low f_{Cl}/f_+ at high DC bias duty cycles, a nearly complete suppression could occur, in which case the PAE yield is close to zero. The red curve in Fig. 8 represents the relative PAE yield with these limits and an intermediate regime that will produce a f_{Cl}/f_+ -independent IAE yield when the modified PAE etching rate is subtracted from the total etching rate to obtain the IAE yield as a function of f_{Cl}/f_+ . These corrected IAE yields are given as the \times s in Fig. 8.

A possible mechanism leading to this conclusion could be that ion bombardment suppresses PAE by disrupting the silicon lattice, introducing e-h Shockley-Read-Hall recombination centers. This occurs above a certain (critical) ion dose requiring a minimum duty cycle of the applied DC bias. The end result is a reduction in the concentration of carriers available for chemical reaction on the

surface, and hence a lower PAE rate, pointing to antisynergism between above threshold-energy ions and VUV photons.

To further support this mechanism, the dependence of the total etching rate on the period of the pulsed negative DC bias was examined with 50% duty cycle at high flow rate (Fig. 9). The ion flux, neutral flux, and VUV photon flux are all constant and independent of the pulsing period. If there is no synergism (positive or negative), then PAE and IAE are two completely independent processes, and the total etching rate is the sum of the IAE rate during half the period and the PAE rate over the full period. Hence, the total etching rate should be independent of the bias pulsing period. Instead, the etching rate decreases as the bias period increases. At very short bias periods, the PAE rate must be constant during the period, since the time is too short to alter the state of the surface or degree of damage. From the data in Fig. 9, this condition corresponds to the removal of only about 0.01–0.1 monolayers at the low or high bias voltage. As the pulsing period increases, the increasing energetic ion dose per cycle causes an increase in the degree of damage of the surface, leading to a suppression of PAE and a decrease in the total etching rate, as is observed in the measurements in Fig. 9, consistent with the proposed negative synergism between energetic ions and VUV photons.

Finally, the higher etching rate at high bias duty cycles found at the low flow rate [Fig. 3(a)], compared to that at high flow rate [Fig. 3(b)], neither supports nor rules out the antisynergism between ions and photons suggested by the other results in this study. It appears that ion bombardment at the low flow rate behaves differently than that at the high flow rate. At the low flow rate, the 1000 nm/min etching rate at 90% duty cycle depletes ~20% of the Cl₂ feed gas, while at the high flow rate, the 800 nm/min etching rate at 90% duty cycle consumes only 3%. At the high flow rate, the ions bombarding the Si substrate are expected to be Ar⁺ and Cl⁺. At the low flow rate, SiCl_x⁺ is likely to become important, since the electron impact ionization rate constants (k_x) favor SiCl_x molecular ion formation near $T_e = 1.5$ eV

($k_{Ar}:k_{Cl}:k_{Cl_2}:k_{SiCl_4}:k_{SiCl_2}:k_{SiCl_3}:k_{SiCl} = 1.0:7:20:60:150:205:980$).^{41–44} Energetic molecular ions will fragment into atoms upon impact,⁴⁵ leading to a reduction of the energy per atom and hence less sub-surface penetration. This could reduce the suppression of PAE at the low flow rate and cause an increase in the total etching rate, and a falloff from linearity at higher bias duty cycles, provided that the IAE rate does not drop off correspondingly.

IV. SUMMARY AND CONCLUSIONS

In this work, p-type Si etching was studied in an RF high density inductively coupled plasma, with Cl₂(10%)/Ar(90%) mixed gas feed at 60 mTorr. A Faraday shield was used to prevent capacitive coupling to the plasma so that the ion energy could be precisely controlled especially on the low energy end, due to a very low plasma potential (~5 V).^{3,4} Real-time etching rates were measured *in situ* by laser interferometry for both PAE with the sample on a grounded substrate stage and IAE with either RF or pulsed negative DC bias applied to the substrate stage. The Si surface chemical composition after etching was determined by vacuum-transfer XPS, and PAE was compared to IAE. Possible synergy between VUV photons and energetic (above threshold-energy) ion bombardment was investigated by varying the duty cycle and period of the pulsed negative DC bias applied to the substrate stage.

Etching rates under pulsed negative DC bias (with a pulsing frequency of 10 kHz and 50% duty cycle) showed an IAE threshold of ~25 eV for the low chlorine flow rate and ~36 eV for the high chlorine flow rate. The subthreshold PAE etching rate was ~300 nm/min for the low flow rate and ~400 nm/min for the high flow rate. Above the threshold, the etching rate scaled linearly with $E^{1/2}$, where E = ion energy. Etching rates measured with RF bias did not show an energy threshold due to the bimodal IED.

XPS measurements showed excellent agreement with the relative chlorine concentration determined using low resolution survey spectra, high resolution Si(2p) spectra, and the corresponding deconvoluted spectra. Most importantly, under PAE conditions (with VUV photons and only subthreshold ions bombarding the surface), the chlorine content was significantly lower, compared to that under IAE conditions, and the chlorinated layer contained only SiCl. Under IAE conditions (with both VUV photons and above threshold-energy ions bombarding the surface), the chlorinated layer contained silicon dangling bonds (Si•), SiCl₂, and SiCl₃ in addition to SiCl, with relative abundance of SiCl > SiCl₂ > SiCl₃. The missing higher chlorides and Si dangling bonds under PAE conditions suggested that, in contrast to VUV photons, energetic ions are more capable of disrupting multiple Si–Si bonds, promoting reactions between Si and adsorbed chlorine leading to higher chlorides. Under IAE conditions, the relative chlorine concentration increased with increasing bias voltage on the substrate stage, as the thickness of the reactive chlorinated layer also increased.

The IAE rate and the energetic ion dose per cycle (with pulsed negative DC bias applied on the sample stage) were closely correlated, increasing linearly with the duty cycle, but only at low duty cycles. Above a certain duty cycle (30% for low flow rate and 20% for high flow rate), as the duty cycle increased, the IAE rate fell below the straight line and the IAE apparent yield decreased with increasing chlorine coverage on the surface. This unreasonable

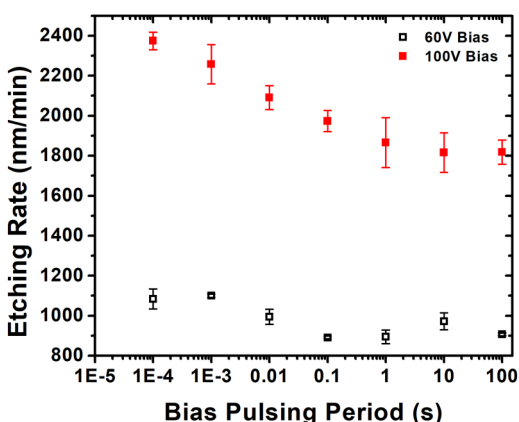


FIG. 9. Total etching rate (sum of IAE and PAE) as a function of pulsed DC bias period with 50% duty cycle, and for negative bias voltage of 60 V (open black square) and 100 V (solid red square), at the high flow rate.

trend of IAE yield indicated that the assumption of PAE rate being constant with increasing duty cycle is not valid and suggested the existence of negative synergy (antisynergism) between VUV photons and energetic ion bombardment when surface damage reaches a certain (critical) value. This antisynergism was further supported by the observed drop of total etching rate with increasing period of the pulsed DC bias. The underlying mechanism could be that ion bombardment creates Si lattice defects, which act as Shockley–Read–Hall recombination centers for photoelectrons and holes, lowering their respective concentration on the surface, thereby lowering PAE.

ACKNOWLEDGMENTS

This work was supported in part by the National Science Foundation (NSF) (No. PHY-1500518) and the Department of Energy, Office of Fusion Energy Science (No. DE-SC0001939).

APPENDIX: CHARGING OF SiO₂ MASK

The ion flux computed from the ion current density measurements is $f_+ = 1.4 \times 10^{17} \text{ cm}^{-2} \text{ s}^{-1}$. For a parallel-plate capacitor with capacitance C , plate separation d , and plate area A , the charge is

$$Q = CV = \frac{k\epsilon_0 A}{d} V,$$

where ϵ_0 is the permittivity of free space and k is the dielectric constant of SiO₂ (3.9). This charge is a function of time and is determined by the positive ion flux as

$$Q = f_+ A e t,$$

where t is the time and e is the elemental charge. Equating these expressions for Q ,

$$V = \frac{f_+ d e}{k\epsilon_0} t.$$

Assuming $d = 1 \times 10^{-4} \text{ cm}$, one obtains $V = 6.5 \times 10^6 t$. Consequently, SiO₂ charges up from -60 to 0 V in $\sim 10 \mu\text{s}$, so above $\sim 10\%$ duty cycle, the SiO₂ mask will charge up to 0 V potential.

REFERENCES

- ¹J. W. Coburn and H. F. Winters, *J. Appl. Phys.* **50**, 3189 (1979).
- ²J. Chang and J. P. Chang, *J. Phys. D Appl. Phys.* **50**, 253001 (2017).
- ³H. Shin, W. Y. Zhu, V. M. Donnelly, and D. J. Economou, *J. Vac. Sci. Technol. A* **30**, 021306 (2012).
- ⁴W. Y. Zhu, S. Sridhar, L. Liu, E. Hernandez, V. M. Donnelly, and D. J. Economou, *J. Appl. Phys.* **115**, 203303 (2014).
- ⁵S. Sridhar, L. Liu, E. W. Hirsch, V. M. Donnelly, and D. J. Economou, *J. Vac. Sci. Technol. A* **34**, 061303 (2016).
- ⁶H. Okano, Y. Horiike, and M. Sekine, *Jpn. J. Appl. Phys.* **24**, 68 (1985).
- ⁷F. A. Houle, *Phys. Rev. B* **39**, 10120 (1989).
- ⁸W. Sesselmann, E. Hudeczek, and F. Bachmann, *J. Vac. Sci. Technol. B* **7**, 1284 (1989).
- ⁹S. Samukawa, B. Jinnai, F. Oda, and Y. Morimoto, *Jpn. J. Appl. Phys.* **46**, L64 (2007).
- ¹⁰M. Fukasawa *et al.*, *Jpn. J. Appl. Phys.* **51**, 026201 (2012).
- ¹¹M. Fukasawa *et al.*, *Jpn. J. Appl. Phys.* **52**, 05ED01 (2013).
- ¹²D. Nest, D. B. Graves, S. Engelmann, R. L. Bruce, F. Weilnboeck, G. S. Oehrlein, C. Andes, and E. A. Hudson, *Appl. Phys. Lett.* **92**, 153113 (2008).
- ¹³E. Pargon, M. Martin, K. Menguelti, L. Azarnouche, J. Foucher, and O. Joubert, *Appl. Phys. Lett.* **94**, 153113 (2009).
- ¹⁴Z. C. Liu, M. Imamura, A. Asano, K. Ishikawa, K. Takeda, H. Kondo, O. Oda, M. Sekine, and M. Hori, *Appl. Phys. Express* **10**, 086502 (2017).
- ¹⁵P. Tian and M. J. Kushner, *Plasma Sources. Sci. Technol.* **24**, 034017 (2015).
- ¹⁶P. Tian and M. J. Kushner, *Plasma Sources. Sci. Technol.* **26**, 024005 (2017).
- ¹⁷S. Y. Tian, V. M. Donnelly, P. Ruchhoeft, and D. J. Economou, *Appl. Phys. Lett.* **107**, 193109 (2015).
- ¹⁸S. Y. Tian, V. M. Donnelly, and D. J. Economou, *J. Vac. Sci. Technol. B* **33**, 030602 (2015).
- ¹⁹S. D. Athavale and D. J. Economou, *J. Vac. Sci. Technol. B* **14**, 3702 (1996).
- ²⁰V. M. Donnelly and J. A. McCaulley, *J. Vac. Sci. Technol. A* **8**, 84 (1990).
- ²¹V. M. Donnelly, D. L. Flamm, C. W. Tu, and D. E. Ibbotson, *J. Electrochem. Soc.* **129**, 2533 (1982).
- ²²V. M. Donnelly, D. E. Ibbotson, and C. P. Chang, *J. Vac. Sci. Technol. A* **10**, 1060 (1992).
- ²³N. Layadi, V. M. Donnelly, and J. T. C. Lee, *J. Appl. Phys.* **81**, 6738 (1997).
- ²⁴N. Layadi, V. M. Donnelly, J. T. C. Lee, and F. P. Klemens, *J. Vac. Sci. Technol. A* **15**, 604 (1997).
- ²⁵H. Shin, W. Y. Zhu, L. Xu, V. M. Donnelly, and D. J. Economou, *Plasma Sources. Sci. Technol.* **20**, 055001 (2011).
- ²⁶R. J. Hoekstra and M. J. Kushner, *J. Appl. Phys.* **79**, 2275 (1996).
- ²⁷J. P. Chang, J. C. Arnold, G. C. H. Zau, H. S. Shin, and H. H. Sawin, *J. Vac. Sci. Technol. A* **15**, 1853 (1997).
- ²⁸J. P. Chang and H. H. Sawin, *J. Vac. Sci. Technol. A* **15**, 610 (1997).
- ²⁹S. A. Vitale, H. Chae, and H. H. Sawin, *J. Vac. Sci. Technol. A* **19**, 2197 (2001).
- ³⁰M. Balooch, M. Moalem, W. E. Wang, and A. V. Hamza, *J. Vac. Sci. Technol. A* **14**, 229 (1996).
- ³¹N. L. Bassett and D. J. Economou, *J. Appl. Phys.* **75**, 1931 (1994).
- ³²J. A. Levinson, E. S. G. Shaqfeh, M. Balooch, and A. V. Hamza, *J. Vac. Sci. Technol. A* **15**, 1902 (1997).
- ³³S. Qin, M. P. Bradley, P. L. Kellerman, and K. Saadatmand, *Rev. Sci. Instrum.* **73**, 1153 (2002).
- ³⁴M. V. Malyshev, V. M. Donnelly, A. Kornblit, N. A. Ciampa, J. I. Colonell, and J. T. C. Lee, *J. Vac. Sci. Technol. A* **17**, 480 (1999).
- ³⁵J. M. Lane, F. P. Klemens, K. H. A. Bogart, M. V. Malyshev, and J. T. C. Lee, *J. Vac. Sci. Technol. A* **18**, 188 (2000).
- ³⁶C. C. Cheng, K. V. Guinn, V. M. Donnelly, and I. P. Herman, *J. Vac. Sci. Technol. A* **12**, 2630 (1994).
- ³⁷L. J. Whitman, S. A. Joyce, J. A. Yarmoff, F. R. McFeely, and L. J. Terminello, *Surf. Sci.* **232**, 297 (1990).
- ³⁸K. H. A. Bogart and V. M. Donnelly, *J. Appl. Phys.* **86**, 1822 (1999).
- ³⁹K. H. A. Bogart and V. M. Donnelly, *J. Appl. Phys.* **87**, 8351 (2000).
- ⁴⁰V. M. Donnelly and M. V. Malyshev, *Appl. Phys. Lett.* **77**, 2467 (2000).
- ⁴¹S. Ashida and M. A. Lieberman, *Jpn. J. Appl. Phys.* **36**, 854 (1997).
- ⁴²C. Lee, D. B. Graves, and M. A. Lieberman, *Plasma Chem. Plasma Process.* **16**, 99 (1996).
- ⁴³M. V. Malyshev and V. M. Donnelly, *J. Appl. Phys.* **87**, 1642 (2000).
- ⁴⁴S. Ashida, C. Lee, and M. A. Lieberman, *J. Vac. Sci. Technol. A* **13**, 2498 (1995).
- ⁴⁵L. Stafford, O. Langlois, J. Margot, M. Gaidi, and M. Chaker, *J. Vac. Sci. Technol. A* **25**, 425 (2007).